#### 2.A.1: 3.A

# DOUBLY RADIATIVE THERMAL NEUTRON CAPTURE IN <sup>2</sup>H AND <sup>16</sup>O: EXPERIMENT AND THEORY

A. B. McDONALD, E. D. EARLE, M. A. LONE, F. C. KHANNA and H. C. LEE

Atomic Energy of Canada Limited, Chalk River Nuclear Laboratories, Chalk River, Ontario, Canada KOJ 1JO

Received 13 September 1976

Abstract: Measurements and calculations are presented for the cross sections for two-photon emission following thermal neutron capture in  $^2H$  and  $^{16}O$ . Upper limits for  $\sigma_{2\gamma}$  were measured in both cases. For  $^2H$ ,  $\sigma_{2\lambda}=8\pm15~\mu$ b, for  $\gamma$ -rays in the energy region  $700 < E_{\gamma} < 5550$  keV. A detailed three-particle calculation gives  $\sigma_{2\gamma}^{tot}=26$  nb. For  $^{16}O$ , the experimental result is  $\sigma_{2\gamma}=3\pm19~\mu$ b for  $1200 < E_{\gamma} < 2943$  keV. A single-particle, direct-capture calculation for  $^{16}O$  gives  $\sigma_{2\gamma}^{tot}=41$  nb. Contributions from excitation of the giant dipole state of the core change this result by  $\pm16~\%$ . In a separate measurement the total cross section for  $^{16}O(n, \gamma)^{17}O$  was measured to be  $202\pm28~\mu$ b. Branching ratios of  $(82\pm3)\%$  and  $(18\pm3)\%$  were determined for decays to the 3055 and 871 keV levels of  $^{17}O$ , respectively.

Е

NUCLEAR REACTIONS  $^{2}$ H(n,  $\gamma\gamma$ ),  $^{16}$ O(n,  $\gamma\gamma$ ),  $^{16}$ O(n,  $\gamma$ ), E = th; measured  $\sigma_{\gamma}$ , deduced upper limit for  $\sigma_{2\gamma}$ .  $^{17}$ O levels deduced  $\gamma$ -branching. Enriched target.

## 1. Introduction

It has been suggested <sup>1</sup>) that the doubly radiative neutron capture cross section for deuterium may be substantially larger than for hydrogen. In addition, it is known that the singly radiative cross section is strongly suppressed due to the symmetry properties of the ground state <sup>2</sup>). The resultant branching ratio,  $\sigma_{2\gamma}/\sigma_{1\gamma}$  could be much more accessible to measurement <sup>3</sup>) than that for hydrogen.

The present paper presents the results of detailed three-body calculations which predict a two-photon emission cross section for deuterium of 26 nb, about four times smaller than that calculated <sup>4</sup>) for hydrogen, 118 nb. In order to understand the smaller cross section for deuterium, a simplified direct capture calculation is described, in which the deuteron is considered to be an elementary particle. It is shown that the statistical and spectroscopic factors and the effective charge all contribute to reduce  $\sigma_{2\gamma}(^2H)$ , even though the phase space is larger. Nevertheless, the calculated branching ratio,  $5 \times 10^{-5}$  is substantially larger than that for hydrogen,  $3.7 \times 10^{-7}$ .

This simplified approach has been used <sup>5</sup>) to calculate  $\sigma_{2\gamma}$  for a number of other cases in which the structure of the target nucleus is well known and  $\sigma_{1\gamma}$  is relatively small. The present work also provides a detailed description of the calculation for <sup>16</sup>O. A value of 41 nb is obtained, corresponding to a branching ratio of  $2.2 \times 10^{-4}$ . It is

shown that direct capture is the dominant capture mechanism and that the result obtained is accurate to within  $\pm 30\%$ .

Experimental results are presented for initial measurements of the two-photon cross sections for deuterium and  $^{16}$ O. Upper limits of  $8\pm15~\mu b$  and  $3\pm19~\mu b$ , respectively, are obtained. These limits are significantly larger than the calculated cross sections. However, an increased neutron flux and better background conditions can be expected to improve the experimental sensitivity in future measurements.

## 2. Theory for doubly radiative <sup>2</sup>H capture

The total doubly radiative capture cross section <sup>6</sup>) is

$$\sigma_{2\gamma} = \frac{1}{2} \frac{2J_{i} + 1}{2(2J + 1)} v_{n}^{-1} \int \frac{d^{3}\omega_{1}}{(2\pi)^{3}} \frac{d^{3}\omega_{2}}{(2\pi)^{3}} \frac{d^{3}p_{f}}{(2\pi)^{3}} \times (2\pi)^{4} \delta(E_{i} - E_{f} - \omega_{1} - \omega_{2}) \delta^{3}(p_{i} - p_{f} - \omega_{1} - \omega_{2}) \sum' |M_{2\gamma}|^{2},$$
 (1)

where the factor  $\frac{1}{2}$  normalises the two-photon final state;  $J_i(J)$  is the spin of the initial state of the total system (target nucleus); the factor 2(2J+1) is the spin statistical weight;  $v_n^{-1} = 1.37 \times 10^5$  is the inverse velocity for thermal neutrons;  $\sum'$  sums over the polarisation of the photons and the magnetic substates of the final state and averages over those of the angular momentum coupled initial state. We use units  $\hbar = c = 1$ . In eq. (1),  $M_{2\gamma}$  is the two-photon matrix element defined as

$$M_{2\gamma} = \left\langle \mathscr{E}_{1q}(\omega_1) \frac{1}{E_i - H} \mathscr{E}_{1q'}(\omega_2) + (1 \rightleftharpoons 2) \right\rangle_{f_i}, \tag{2}$$

where H is the sum of the nuclear Hamiltonian for the three-nucleon system and the free electromagnetic field, and  $\mathscr{E}_{1o}(\omega)$  is the electric dipole operator <sup>4</sup>)

$$\mathscr{E}_{1q}(\omega) = -ie\sqrt{\frac{3}{2\omega}} \int d\Omega_{\omega} Y_{1q}(\hat{\omega}) e^{i\omega \cdot r}$$
 (3)

in a co-ordinate frame chosen such that the z-axis is along the momentum vector  $\omega$  of the photon. This form of the matrix element is obtained by using the method of Grechukhin <sup>6</sup>) which eliminates the linear dependence of the dipole operator on the photon energy. In the long wavelength approximation ( $\omega r \ll 1$ ), this operator reduces to the conventional dipole operator

$$\mathscr{E}_{1q}(\omega) = e \sqrt{\frac{2\pi}{\omega}} \, \omega \mathbf{s}_q \cdot \mathbf{r}. \tag{4}$$

Based on the results for n<sup>1</sup>H capture <sup>4</sup>), we have assumed in this calculation that the (E1, E1) two-photon mode is dominant and all other two-photon modes have been ignored.

## 2.1. THE FINAL STATE

The final n<sup>2</sup>H state, or the triton, is described by the wave function <sup>2</sup>)

$$\psi = c_0 w_{00} \phi_0 + c_s (w_{1,0} \phi_1 + w_{2,0} \phi_2) + c_A w_{3,0} \phi_3 + d_s (w_{1,2} \psi_1 + w_{2,2} \psi_2), \tag{5}$$

where  $\phi_1$  and  $\phi_2$  are the partially symmetric, and  $\phi_0$  and  $\phi_3$  respectively the completely antisymmetric and completely symmetric spin and isospin functions of the three nucleons with total spin  $S=\frac{1}{2}$  and isospin  $T=\frac{1}{2}$ ;  $\psi_1$  and  $\psi_2$  are respectively antisymmetric and symmetric in the isospin space under the exchange of particles 2 and 3 and have  $S=\frac{3}{2}$  and  $T=\frac{1}{2}$ . The normalized spatial functions  $w_{i,L}$  (with orbital angular momentum L) are chosen with appropriate symmetry properties such that  $\psi$  is completely antisymmetric and normalised. The magnitude of the constants  $c_0$ ,  $c_s$ ,  $c_A$  and  $d_s$  can be obtained from detailed calculations of the ground-state properties of the three-nucleon system. Such calculations  $^{7,8}$ ) give approximately  $|c_0|^2 \approx 0.90$ ,  $|c_s|^2 \approx 0.016$ ,  $|c_A|^2 \approx 0.0005$  and  $|d_s|^2 \approx 0.09$ .

Due to the fact that the L=2 component in the initial state arises only through the D-state component in the deuteron and the consideration that the spin and isospin symmetries are not changed in an E1 transition it can be shown that the first term in eq. (5) dominates the transition over and above the fact that  $|c_0|$  is the largest of the four amplitudes. Therefore for the present calculation, the triton wave function is approximated as

$$\psi \approx c_0 w_{00} \phi_0, \tag{6}$$

where

$$w_{00} = \frac{1}{3} \bar{N}_{i} (h_1 + h_2 + h_3), \qquad h_i = h(\rho_i, R_i), \tag{7}$$

where  $\rho_i = r_j - r_k$ ,  $R_i = r_i - \frac{1}{2}(r_j + r_k)$  and  $R_c = \frac{1}{3}(r_1 + r_2 + r_3)$  with (i, j, k) being cyclic permutations of the particle labels (123) (we designate the neutron in the  $n^2H$  system by label 1). Here  $\bar{N}_f$  is the normalization constant. From the binding energy of the deuteron  $(B_d)$  and the triton  $(B_t)$  we know that asymptotically  $h_i$  has the form

$$h_i = \phi_{d}(\rho_i) \sqrt{2\gamma_1} \frac{e^{-\gamma_1 R_i}}{R_i} Y_{00}(\hat{R}_i), \qquad (8)$$

where  $\gamma_1 = \sqrt{2\mu\omega}$ ,  $\mu = \frac{2}{3}M$  is the reduced mass of the n<sup>2</sup>H system (M is the nucleon mass),  $\omega = B_t - B_d$  is the Q-value for the capture reaction, and  $\phi_d$  is the internal wave function of the deuteron 8)

$$\phi_{d}(\rho) = N_{d} \frac{\sqrt{2\beta_{1}}}{\rho} (e^{-\beta_{1}\rho} - e^{-\beta_{2}\rho}) Y_{00}(\hat{\rho}), \tag{9}$$

where  $|N_d|^2 = 1.69$ ,  $\beta_1 = \sqrt{MB_d}$  and  $\beta_2 = 5.73 \ \beta_1$ . Inside the nucleus,  $h_i$  has to be properly regularised at the origin. We follow Hulthén and Sugawara 9) and choose the form

$$h_i = \phi_d \frac{\sqrt{2\gamma_1}}{R_i} (e^{-\gamma_1 R_i} - e^{-\gamma_2 R_i}) Y_{00}(\hat{R}_i). \tag{10}$$

The radius of the triton requires the magnitude of  $\gamma_2$  to be similar to that of  $\beta_2$ . We shall present results obtained with a range of values of  $\gamma_2$ .

#### 2.2. THE INITIAL STATE

The initial state of the  $n^2H$  system can be in the spin doublet continuum,  $^2S_{\frac{1}{2}}$ , or in the quartet continuum,  $^4S_{\frac{1}{2}}$ . Since the electric dipole operator cannot change the spin in a transition from the initial to the final state which is more than 90% spin doublet, we need only consider the initial state in the doublet continuum. Because the deuteron has zero isospin the initial state must have  $T = \frac{1}{2}$ . The wave function for such a state is chosen to have the form

$$\psi_{\rm sc} = \phi_{\rm d}(\rho_1)(1 - a_2/R_1)Y_{00}(\hat{R}_1)S_{\sigma}A_{\rm p} \tag{11}$$

where  $S_{\sigma}$  and  $A_{\tau}$  are respectively symmetric in spin space and antisymmetric in isospin space with respect to the interchange of particles 2 and 3. In (11)  $a_2 = 0.65$  fm is the scattering length <sup>7</sup>) for the n<sup>2</sup>H system in the doublet state.

## 2.3. TWO-PHOTON CROSS SECTION

Using plane-wave intermediate states, the two-photon matrix element  $M_2$  is written as

$$M_{2y} = 2\pi\alpha\sqrt{\omega_1\omega_2}\mathbf{s}_1 \cdot \mathbf{s}_2(f_{2y}(x) + f_{2y}(1-x)), \tag{12}$$

where  $\alpha = \frac{1}{137}$  is the fine structure constant,  $\epsilon_1$  and  $\epsilon_2$  are the polarisations of the two photons,  $x = \omega_1/\omega$  and a detailed expression for the function  $f_{2\gamma}(x)$  is given in appendix A. The differential cross section for two-photon capture is given by

$$d\sigma_{2\gamma} = \frac{1}{6\pi} \frac{\alpha^2}{v_n} (1 + \cos^2 \theta) d(\cos \theta) \omega_1^3 (\omega - \omega_1)^3 d\omega_1 |f_{2\gamma}(x) + f_{2\gamma}(1 - x)|^2,$$
 (13)

where  $\theta$  is the angle between the direction of the two photons with energy  $\omega_1$  and  $\omega_2$ . The integrated cross section is given by

$$\sigma_{2\gamma} = \frac{4}{9\pi} \frac{\alpha^2}{v_n} \omega^7 \int_0^1 x^3 (1-x)^3 |f_{2\gamma}(x) + f_{2\gamma}(1-x)|^2 dx.$$
 (14)

#### 2.4. NUMERICAL RESULTS

The total cross section for two photon emission, using the initial state wave function given by eq. (11) and the final state wave function given by eqs. (7), (9) and (10), is shown in table 1 in which magnitude of  $\gamma_2$  is varied and results for several values of  $\gamma_2$  are shown. The value  $\gamma_2 = 3.5 \gamma_1$  (or  $\gamma_2 = 307 \text{ MeV/c}$ ) reproduces the radius <sup>7</sup>) of <sup>3</sup>H reasonably well and provides a type of phenomenological wave function <sup>10</sup>)

$\gamma_2/\gamma_1$	$ \bar{N}_{\mathrm{f}} ^2$	$\sqrt{\langle r^2 \rangle}$ (fm)	$\sigma_{2_{7}}^{\delta}$ (nb)	$\sigma_{2\gamma}^{\rm tot}$ (nb)
1.5	14.0	2.14	60.5	58.3
2.0	5.62	2.02	43.0	41.3
2.5	3.68	1.92	34.8	33.3
3.0	2.87	1.86	30.2	28.8
3.5	2.44	1.82	27.2	26.0
4.0	2.18	1.79	26.0	24.7

TABLE I  $\sigma_2$ , for  $n^2H$  capture

that gives a good fit to the charge form factor of  ${}^3H$  for momentum transfers up to 3.5 fm $^{-1}$ . For this choice of  $\gamma_2$ , the square of the asymptotic normalisation,  $|\bar{N}_f|^2 = 2.44$ , has a value consistent with those obtained by others  ${}^7$ ). The column  $\sigma_{2\gamma}^b$  ( $\sigma_{2\gamma}^{tot}$ ) gives the two-photon cross section ignoring (including) the term in the initial state wave function proportional to  $a_2$ . Since  $a_2$  is small, the term proportional to  $a_2$  changes the cross section by only  $\approx 4 \%$ . For a realistic choice of  $\gamma_2 \approx 300$  MeV/c, the total two-photon cross section is 26.0 nb. The curve labeled (a) in fig. 1 shows the calculated two-photon spectrum. As in the case of  ${}^1H(n,\gamma\gamma)^2H$ , where the cross section was shown to be insensitive to the internal region of the deuteron wave function, here the cross section is also not sensitive to the relative  $n^2H$  wave function at short distances. For example if we set  $\gamma_2 = \infty$ , i.e. using the asymptotic wave function given in (8), but the normalization  $|\bar{N}_f|^2 = 2.44$ ,  $\sigma_{2\gamma}$  becomes 30.1 nb, representing an increase of 16 %.

The remaining uncertainty in the results arises from the effect of interaction in the plane wave intermediate states. Since the p-wave phase shift is small at low energies, this effect is not expected to be important. For  $n^1H$  capture 4) this effect changes the cross section by much less than 1%.

We calculate  $\sigma_{2\gamma}$  to be 26 nb with an estimated uncertainty of about 30%.

#### 2.5. COMPARISON WITH THE RESULT OF 1H CAPTURE

It has been suggested 1) that because of the larger phase space  $\sigma_{2\gamma}(^2H)$  could be an order of magnitude larger than  $\sigma_{2\gamma}(^1H)$ . In the previous section we have shown instead that  $\sigma_{2\gamma}(^2H)$  is smaller by a factor of four. This result can be understood by means of a simplified calculation in which the deuteron is considered to be an elementary particle. In this case the formalism 4) for neutron capture on hydrogen (using asymptotic wave functions only) can be carried over and we write

$$\sigma_{2\gamma} = S|C|^2 \bar{N}_f^2 \frac{64}{9} \frac{\alpha^2}{v_n} \left(\frac{\omega}{2\mu}\right)^{\frac{4}{3}} \gamma_1^{-2} \left(\frac{Z}{A}\right)^4 (1 - \frac{2}{5}\eta + 0.041\eta^2), \tag{15}$$

where S is the spin-statistics weight factor;  $|C|^2$  is the spectroscopic factor for the

capture process;  $\mu = ((A-1)/A)M$  is the reduced mass of the neutron; A is the mass number of the product nucleus;  $\omega (= B_t - B_d)$  is the total photon energy; -Z/A is the neutron effective charge in units of e and  $\eta = a_2 \gamma_1$  where  $\gamma_1 = \sqrt{2\mu\omega}$ . Table 2 compares the values of S,  $|C|^2$ , etc. for the  $n^1H$  and  $n^2H$  cases. It can clearly be seen that the value of  $\omega$  alone does not have a dominating effect on  $\sigma_{2\gamma}$ . In the case of  $n^2H$  capture, the smaller value of S,  $|C|^2$  and the effective charge all contribute to reduce the cross section.

Table 2

Comparison of n<sup>1</sup>H and n<sup>2</sup>H capture

	S	C  <sup>2</sup>	$ar{N}_{ m f}^2$	$\mu/M$	Z/A	ω (MeV)	$\gamma_1$ (fm <sup>-1</sup> )	η
n¹H n²H	3 4 1 3	1 1 2	1.69 2.44	1 2 2 3	1 1 3	2.22 6.26	0.232 0.449	1.25 0.292

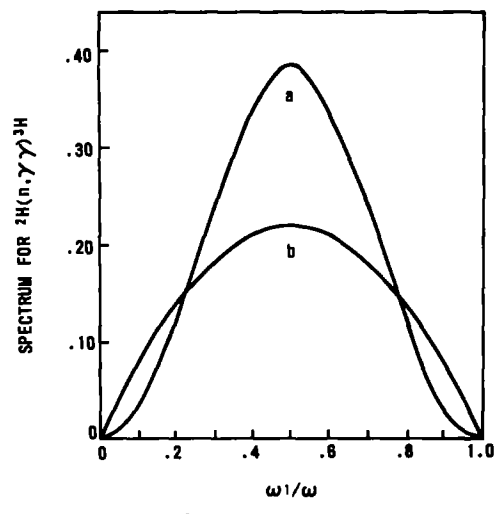


Fig. 1. Predicted two-photon spectra for <sup>2</sup>H(n, γγ)<sup>3</sup>H, in dimensionless units; (a) obtained from three-body calculation; and (b) obtained from two-body calculation.

The result obtained with eq. (15),  $\sigma_{2\gamma}(^2H) = 20.3$  nb is remarkably close to the value of 26 nb obtained from the three-body calculation. The contribution of the internal structure of the deuteron to  $\sigma_{2\gamma}(^2H)$  is not expected to be large because the relative wave function of the  $n^2H$  system in the bound state is orthogonal to the relative  $n^2H$  scattering wave function. However, as is shown in fig. 1, there is a qualitative difference between the two-photon spectra obtained from the two calculations. At  $\omega_1 \approx 0$  or  $\omega_1 \approx \omega$ , the linear dependence on  $\omega_1$  of the capture rate is characteristic of two-body capture only.

# 3. Theory for doubly radiative n<sup>16</sup>O capture

The single-particle plus core picture used in the last section is expected to be increasingly realistic as the mass of the target nucleus increases. Closed shell nuclei are particularly attractive because the wave functions of the single particles are well known. The nucleus  $^{16}$ O provides the additional advantages that there is no resonance at or near thermal neutron energy and  $\sigma_{1\gamma}$  is relatively small. The capture mechanism described in subsect. 2.5 is therefore expected to be the dominant contribution to  $\sigma_{2\gamma}$ . The only other capture mechanisms which we consider are those due to the giant-dipole resonance (GDR).

Because the ground state of <sup>17</sup>O has  $J^{\pi} = \frac{5}{2}^{+}$  the final neutron state must be in a bound, d-wave orbital. The  $\sigma_{2y}$  can be written as (see appendix B)

$$\sigma_{2\gamma} = \bar{N}_{\rm f}^2 \frac{160}{3} \frac{\alpha^2}{v_{\rm p}} \left(\frac{\omega}{2\mu}\right)^{\frac{4}{3}} \gamma_1^{-2} \left(\frac{Z}{A}\right)^4 F(\eta). \tag{16}$$

In comparison with (15) we note that here both S and  $|C|^2$  are equal to unity. The function  $F(\eta)$  is defined as

$$F(\eta) = 6 \int_0^1 |f(x) + f(1-x)|^2 x^3 (1-x)^3 dx, \tag{17}$$

where the dimensionless, reduced two-photon amplitude f(x) is

$$f(x) = f^{s.p.}(x) + f^{GDR}(x) + f^{2+}(x), \tag{18}$$

where

$$f^{\text{a.p.}}(x) = \frac{1}{15} \frac{1}{x} \int_0^\infty u_2(z) z^4 dz - \frac{4\eta}{\pi} \int_0^\infty \frac{dp}{(p^2 + x)p} \left[ 1 - \left( \frac{p^2}{p^2 + \zeta^2} \right)^2 \right] \int_0^\infty u_2(z) z^3 j_1(pz) dz$$
(19)

is due to single-particle direct capture;

$$|f^{GDR}(x)| = \frac{y_d}{\sqrt{90}} \frac{K}{\bar{N}_f} \sqrt{\frac{AN}{Z}} \frac{1}{\sqrt{x_D}} \frac{1}{x_D + x}$$
 (20)

is due to direct capture through core-excited intermediate states; and

$$f^{2+}(x) \approx 2f^{GDR}(x) \tag{21}$$

is due to the initial  $(\frac{1}{2}^+)$  and the final  $(\frac{5}{2}^+)$  states having components  $|(1^-\otimes 1^-)2^+d_5;\frac{1}{2}^+\rangle$  and  $|(1^-\otimes 1^-)2^+s_1';\frac{5}{2}^+\rangle$  respectively. Here  $d_5$  is the final, bound d-wave in  ${}^{17}$ O,  $s_1'$  is the initial scattering s-wave of the thermal neutron, and  $|1^-\rangle$  is the GDR. In (19),  $u_2$  is the radial wave function for  $d_5$  generated from a Woods-Saxon potential  ${}^{11}$ )  $(N_f^2 \int_0^\infty u_2^2 r^2 dr$  is normalized to unity;  $N_f^2 = 2\gamma_1 \bar{N}_f^2$ ) and the term  $[p^2/(p^2 + \zeta^2)]^2$  arises from the regularization of the initial scattering s-wave,  $u_0(r) = 1 - (\eta \gamma_1/r)(1 - e^{-\zeta \gamma_1 r})$ . In (20),  $y_d$  is the amplitude of the particle-hole com-

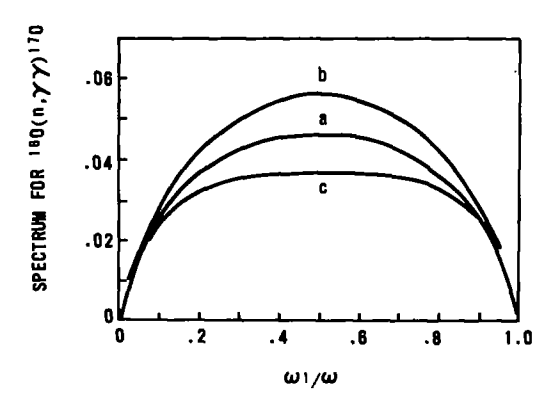


Fig. 2. Predicted two-photon spectra for  $^{16}O(n, \gamma \gamma)^{17}O$ . (a) Calculated from  $f^{n,p}$  only; (b) calculated from  $|f^{n,p}| + |f^{GDR} + f^{2^+}|$ ; and (c) calculated from  $|f^{n,p}| - |f^{GDR} + f^{2^+}|$ .

ponent  $(d_5p_3^{-1})$  in the GDR;  $K\gamma_1^{-\frac{4}{3}}$  is equal to the radial integral in the electric dipole transition  $s_1'$  to  $p_3$ ; and  $x_D = \omega_D/\omega$ , where  $\omega_D$  is the excitation energy of the GDR.

The two-photon spectrum labeled a in fig. 2 is calculated using  $f^{*,p}$  only. With  $\zeta=0.6$ , or  $\zeta\gamma_1$  being approximately the nuclear radius, the integrated  $\sigma_{2\gamma}$  is 41 nb. No attempt has been made to predict the relative sign between the amplitudes  $f^{*,p}$  and  $f^{GDR}+f^{2^+}$ . The spectrum labeled b (c) in fig. 2 is obtained when these amplitudes are added constructively (destructively); the corresponding  $\sigma_{2\gamma}$  is 48 nb (34 nb). In short, including the effect of the GDR changes the result of single-particle direct capture by  $\pm 16\%$ . Together with the uncertainty of the wave function of  $s_1'$  in the nuclear interior, the total uncertainty for the value  $\sigma_{2\gamma}=41$  nb is about  $\pm 30\%$ . The results are summarized in table 3.

TABLE 3  $\sigma_{2\gamma}$  for n<sup>16</sup>O capture

			Single-particle	(.1)	
ω (MeV	a (fm)	$\bar{N}_t^2$	$u_2 = u_2^{\text{asym}}$ $\zeta = \infty$	$\zeta = 0.6$	σ <sub>2γ</sub> (nb) total
4.14	5.81 *)	0.705	36	41	48 b) 34 °)

a) Ref. 12).

b) The amplitudes  $f^{s,p}$  and  $f^{GDR} + f^{2+}$  are added constructively.

<sup>&</sup>lt;sup>e</sup>) The amplitudes are added destructively.

## 4. Experiment

The apparatus and techniques used in the present experiment were similar to those used in a previous measurement 3) of an upper limit for  $\sigma_{2\gamma}(^{1}H)$ .

The experiment was performed with 0.009 eV neutrons obtained by Bragg reflecting a beam of neutrons from the NRU reactor thermal column with a pyrolitic graphite monochromator. The beam  $(4\times10^5$  neutrons cm $^{-2}\cdot s^{-1})$  travelled down a 4 cm inside diameter flight tube lined with 5 mm of <sup>6</sup>LiF to a 50 cm<sup>3</sup> sample of heavy water (99.76% isotopically enriched in <sup>2</sup>H) contained in a bag made of 0.1 mm thick polyethylene. Since the scattering cross section for deuterium is 500 times the capture cross section <sup>12</sup>), the neutron beam was effectively thermalized to 0.025 eV in the target before capture. The use of a <sup>2</sup>H<sub>2</sub>O target permitted the simultaneous measurement of two-photon emission cross sections from <sup>2</sup>H and <sup>16</sup>O.

The  $^6$ LiF shielded the detectors from neutrons in the beam and neutrons scattered from the target, providing a linear attenuation factor of greater than  $10^{10}$  for thermal neutrons. Two Ge(Li) detectors having photopeak efficiencies of 11.3 % and 13.3 % at 1.33 MeV (relative to a 7.6 cm  $\times$  7.6 cm NaI detector at 25 cm) were placed as close

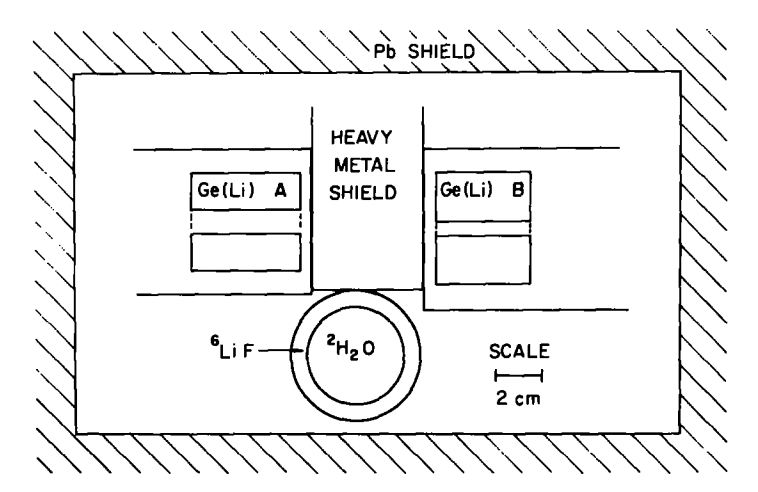


Fig. 3. Target-detector configuration used in the present experiment. The neutron beam travelled perpendicular to the plane of the figure within an extended <sup>6</sup>LiF tube.

to the target as possible (fig. 3) and were shielded from each other by 4.9 cm of heavy metal. In addition, the target-detector assembly was surrounded by 10 cm of Pb.

A PDP-5 computer was used on line to store on magnetic tape three-parameter events consisting of the energy signals from each detector and a fast timing signal from a time-to-amplitude converter (TAC). The fast-coincidence time resolution was about 6 ns FWHM and was achieved by using two ORTEC 473 constant fraction discriminators in a slow-rise-time-rejection mode. Large amplitude pulses from a mercury relay pulser were fed in at each preamplifier and the resulting signals

were used for gain stabilization during playback of the data on a PDP-10 computer.

During the acquisition of the data, singles energy spectra from detector A were accumulated in a 1024 channel analyzer, and the number of counts in the 2223 keV line from the  $^{1}$ H(n,  $\gamma$ ) reaction was scaled in a 10 MHz scaler to monitor the beamtarget interactions.

Relative detection efficiencies in the energy range from 1 to 10 MeV were determined from the known  $^{13-15}$ ) intensities of  $\gamma$ -rays from  $(n, \gamma)$  reactions in nitrogen, carbon and lithium. Relative efficiencies at lower energies were determined with radioactive sources of  $^{22}$ Na,  $^{88}$ Y and  $^{60}$ Co dissolved in volumes of  $H_2$ O similar to that of the  $^2H_2$ O target.

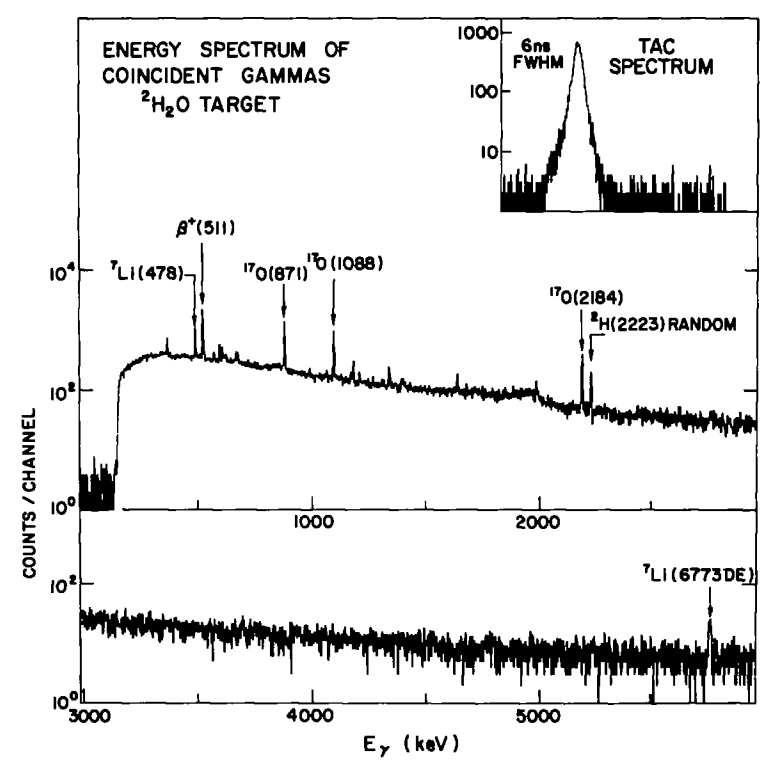


Fig. 4. Energy spectrum of  $\gamma$ -rays in detector A in coincidence with any  $\gamma$ -ray in detector B. The insert shows a typical spectrum from the time to amplitude converter (TAC).

Fig. 4 shows the spectrum of energy pulses observed in detector A in real coincidence with pulses of any energy in detector B. The insert illustrates a typical TAC spectrum.

The experimental difficulties in the present measurements were significantly different from those associated with the  ${}^{1}H(n, \gamma\gamma){}^{2}H$  measurement  ${}^{3}$ ). In the present case, the flux of  $\gamma$ -rays from single photon emission in the target is lower by a factor

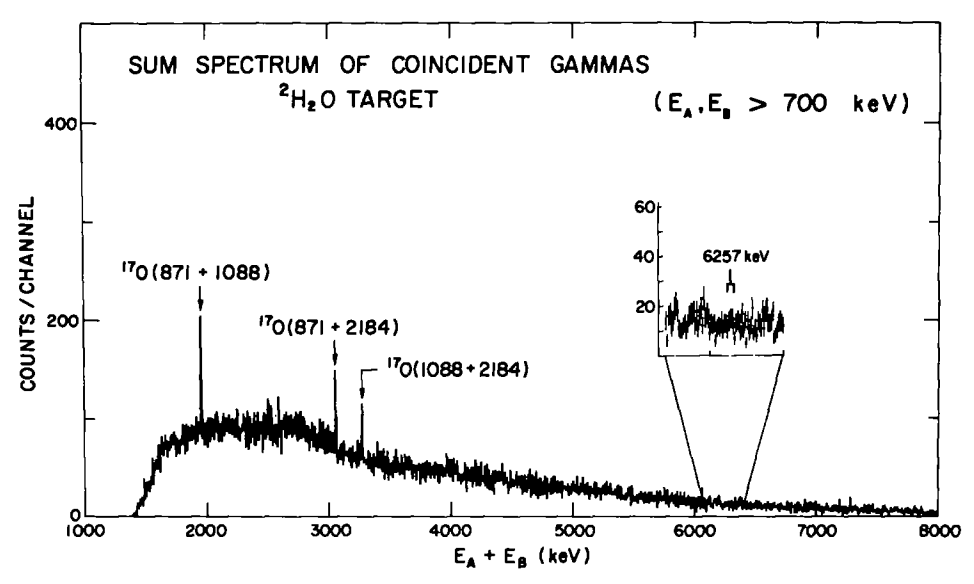


Fig. 5. Sum spectrum obtained with the  $^2H_2O$  target for a total accumulation time of 300 hours. The energies of the  $\gamma$ -rays in detectors A, B have been restricted to the range  $E_A$ ,  $E_B > 700$  keV. The peaks arise from cascade  $\gamma$ -rays from the  $^{16}O(n, \gamma)^{17}O$  reaction. The insert indicates the region summed to determine  $\sigma_{2\gamma}$  for deuterium.

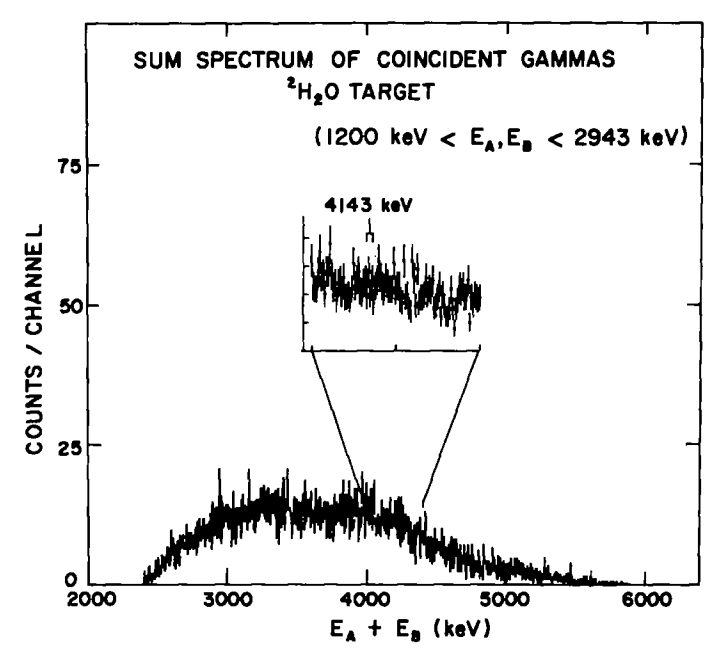


Fig. 6. Sum spectrum obtained as in fig. 5, but with  $1200 < E_A$ ,  $E_B < 2943$  keV. The insert indicates the region summed to determine  $\sigma_{2\gamma}$  for oxygen.

of more than 600. Therefore, the problem of cross registration of  $\gamma$ -rays is much less significant. The lower singles counting rates (< 100/s) also result in a very low random coincidence rate (see TAC spectrum in fig. 4).

The main source of background is real coincidences between the Compton distribution of high-energy  $\gamma$ -rays produced by  $(n, \gamma)$  reactions in materials other than the deuterium in the target. By comparing the discrete  $\gamma$ -ray lines apparent in fig. 4 with  $(n, \gamma)$  spectra obtained from a variety of targets it was possible to identify background contributions from  $(n, \gamma)$  reactions in hydrogen (random coincidences), oxygen, nitrogen, carbon, fluorine, germanium, lithium and cadmium. Much of this background is produced by  $\gamma$ -ray coincidences having at least one  $\gamma$ -ray less than 700 keV and this background was digitally rejected during data playback. The main contribution to background in the regions of interest arose from  $(n, \gamma)$  reactions in nitrogen and germanium, with additional small contributions from fluorine and cadmium. The contributions from the former two sources were reduced by filling the neutron flight tube with helium and by minimizing the leakage of neutrons out of the tube.

During data playback, sum spectra were generated from the coincident signals from the two detectors for various energy ranges. Figs. 5 and 6 show the sum spectra obtained with the restrictions  $E_A$ ,  $E_B > 700$  keV and  $1200 < E_A$ ,  $E_B < 2943$  keV, respectively. The former energy discrimination was chosen primarily to reject events due to cross registration from positron annihilation at rest. The higher threshold (1200 keV) was necessary for the  $\sigma_{2\gamma}(^{16}O)$  measurement to reject contributions from two-step cascades via known  $^{17}O$  levels.

The spectrum of fig. 5 was used to determine an upper limit for  $\sigma_{2\gamma}(^2H)$ . As may be seen in the insert, no peak was observed at 6257 keV and the net yield in a region of 14 keV at that energy was determined to be  $4.5\pm8.3$  counts. The energy calibration and resolution were determined from the singles spectra and the sum spectra observed for the  $^{14}N(n, \gamma)$  and  $^{12}C(n, \gamma)$  reactions.

From measurements performed with the heavy metal shield removed, the contribution from cross registration <sup>16</sup>) of 6257 keV  $\gamma$ -rays from the <sup>2</sup>H(n,  $\gamma$ )<sup>3</sup>H reaction was calculated to be negligible. As in the previous measurement <sup>3</sup>) of  $\sigma_{2\gamma}(^{1}H)$  the clearly resolved peaks in fig. 5 due to the coincident cascade  $\gamma$ -rays from the <sup>16</sup>O(n,  $\gamma$ ) reaction were used as an absolute normalization in determining  $\sigma_{2\gamma}(^{2}H)$ . Corrections of less than 3 % were applied for contributions from oxygen in the polyethylene bag and the residual  $^{1}H_{2}O$  in the  $^{2}H_{2}O$  sample.

The coincidence data obtained in the course of the present measurement (fig. 5) were used to define branching ratios of  $(18\pm3)\%$  and  $(82\pm3)\%$  for the decays to the 871 and 3055 keV levels of <sup>17</sup>O (see fig. 7). Singles spectra (fig. 8) were also obtained in which  $\gamma$ -rays of energies  $870.89\pm0.22$ ,  $1087.88\pm0.17$ ,  $2184.47\pm0.12$  and 3271 keV were observed and their intensities were determined relative to the intensity of the 6257 keV  $\gamma$ -ray from <sup>2</sup>H(n,  $\gamma$ )<sup>3</sup>H for which  $\sigma = 521\pm9~\mu b$  [ref. <sup>17</sup>)]. Using the measured branching ratios and relative efficiencies of the detectors, the total cross

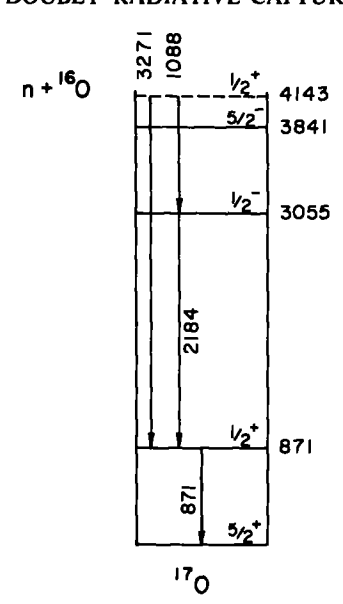


Fig. 7. Energy level diagram showing the transitions observed from the  $^{16}O(n, \gamma)$  reaction. Energies are shown in keV.

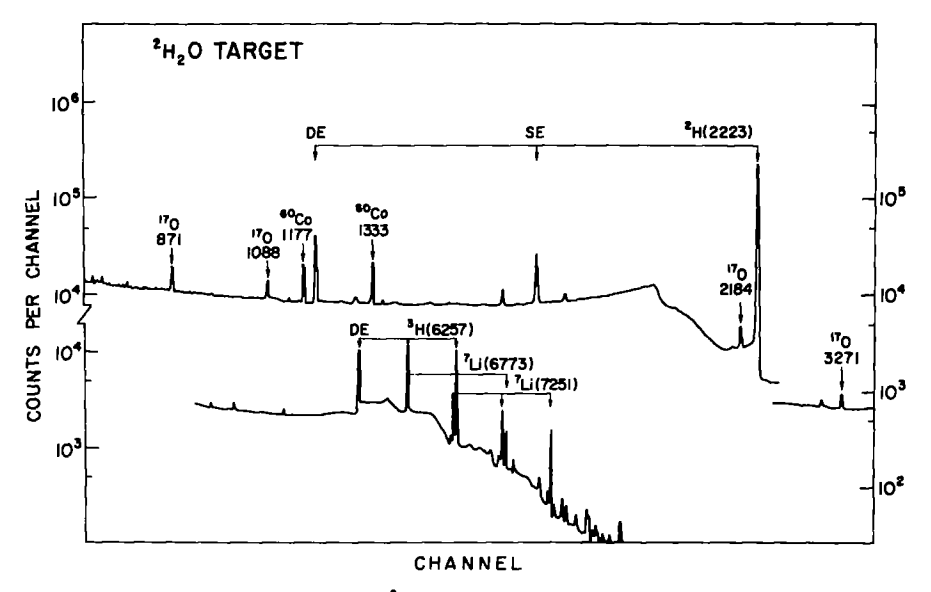


Fig. 8. Singles spectrum of  $\gamma$ -rays from the  $^2H_2O$  target, used to determine the cross section and branching ratios for  $^{16}O(n, \gamma)$ . The peaks labelled DE and SE are double and single escape peaks, respectively.

section for the  $^{16}\text{O}(n, \gamma)$  reaction was determined to be  $202 \pm 28 \ \mu\text{b}$ . These results are in agreement with the results of Jurney and Motz  $^{18}$ ) who measured branching ratios of 82 and 18 % and a total cross section of  $178 \pm 25 \ \mu\text{b}$ . The weighted average of these cross-section measurements is  $190 \pm 18 \ \mu\text{b}$ .

These <sup>17</sup>O results and the measured relative  $\gamma$ -ray detection efficiencies were used to define the cross section for <sup>2</sup>H(n,  $\gamma\gamma$ )<sup>3</sup>H for  $700 < E_{\gamma} < 5557$  keV:

$$\sigma_{2\nu}(^{2}\text{H}) = 8 \pm 15 \ \mu\text{b}.$$

This corresponds to a two-photon branching ratio  $\sigma_{2\gamma}/\sigma_{1\gamma}$  of  $(1.5\pm2.8)\times10^{-2}$ . The average detection efficiency for the  $2\gamma$  process in  $^2H$  was determined by assuming a two-photon energy distribution as shown in fig. 1 (curve a). However,  $\sigma_{2\gamma}(^2H)$  is not very sensitive to this distribution, since a form independent of  $E_{\gamma}$  would only increase the result for  $\sigma_{2\gamma}$  by about 15%. The angular correlation of the two photons from  $^2H(n,\gamma\gamma)$  was assumed to be isotropic. The solid angles subtended by the two Ge(Li) detectors are so large that the expected (see sect. 2) angular dependence for an E1-E1 transition  $(1+\cos^2(\theta_A-\theta_R))$  would change this result by less than 10%.

The sum spectrum of fig. 6 was used to determine an upper limit for  $\sigma_{2\gamma}(^{16}\text{O})$ . The somewhat large energy limit of 1200 keV was chosen to reduce the background in the region of interest. In particular, this choice eliminates contributions from two-step cascades via known <sup>17</sup>O levels. A possible contribution from the triple coincidence (871 + 1088 + 2184 keV) is calculated to be negligible in this experiment. It could always be eliminated completely by rejecting a small energy region near 2184 keV in each detector.

As shown in the insert in fig. 6, no peak was observed at 4143 keV and the net counts in a region of 12 keV were determined to be 1.5  $\pm$  7.5. Again, by normalizing to the two-step cascades in <sup>17</sup>O the cross section for <sup>16</sup>O(n,  $\gamma\gamma$ )<sup>17</sup>O was determined for 1200 <  $E_{\gamma}$  < 2943 keV:

$$\sigma_{2\gamma}(^{16}\text{O}) = 3 \pm 19 \ \mu\text{b}.$$

This corresponds to a two-photon branching ratio of  $(1.6\pm10)\times10^{-2}$ . The energy distribution shown in fig. 2 (curve a) was used to define the average detection efficiency. The anisotropy of the two-photon angular correlation is negligible [see eq. (B.1)].

## 5. Summary

The theoretical and experimental values of two-photon emission cross sections and branching ratios for thermal neutron capture by hydrogen, deuterium and  $^{16}$ O are listed in table 4. Although the calculated values of  $\sigma_{2\gamma}$  for  $^{2}$ H and  $^{16}$ O are somewhat smaller than for  $^{1}$ H, the branching ratios are substantially larger.

The experimental upper limits for the cross sections in all cases are of the same

Target	σ <sub>1γ</sub> (μb)	σ <sub>2γ</sub> (calc) (nb)	$\sigma_{2\gamma}/\sigma_{1\gamma}$ (calc)	σ <sub>2γ</sub> (exp) (μb)	$\sigma_{2\gamma}/\sigma_{1\gamma}$ (exp)	Energy range *) (keV)
<sup>1</sup> H	$(3.32\pm0.02)\times10^{5}$ b)	118	$3.6 \times 10^{-7}  5 \times 10^{-5}  2.2 \times 10^{-4}$	-3± 8	$(-0.9\pm2.4)\times10^{-5}$	$600 < E_{\gamma} < 1600$
<sup>2</sup> H	$521\pm9$ °)	26		8±15	$(1.5\pm2.9)\times10^{-2}$	$700 < E_{\gamma} < 5550$
<sup>16</sup> O	$190\pm18$ d)	41		3±19	$(1.6\pm10)\times10^{-2}$	$1200 < E_{\gamma} < 2943$

TABLE 4 Summary of theoretical and experimental results

order. However, the main limitation to the sensitivity 3) for the <sup>1</sup>H case arises from the relatively large  $\sigma_{1}$ , (<sup>1</sup>H). For <sup>2</sup>H and <sup>16</sup>O, the present limitation results from background produced by  $(n, \gamma)$  reactions in materials other than the target. In principle, improvements can be obtained by decreasing this background and by increasing the incident flux.

Until now, essentially all experimental and theoretical work in doubly radiative thermal neutron capture has concentrated on the hydrogen case. The present work indicates that other cases can be calculated with reasonable certainty and that these cases may be more accessible to measurement.

We would particularly like to thank the Solid State Physics Group at CRNL for the use of their monochromator facility.

# Appendix A

The function  $f_{2\nu}(x)$  corresponding to initial wave functions of the type (suppressing the angular, spin and isospin wave functions)

$$N_{\rm d}\sqrt{2\beta_1}\frac{{\rm e}^{-\beta'\rho_1}}{\rho_1}\,\frac{\sin\left(kR_1+\delta_2\right)}{kR_1},$$

and final wave functions of the type

$$h_i = N_d \sqrt{2\beta_1} \frac{e^{-\beta \rho_i}}{\rho_i} \sqrt{2\gamma_1} \frac{e^{-\gamma R_i}}{R_i}$$

is

$$f_{2\gamma}(x) = \frac{16}{9} \sqrt{\pi} M N_{\rm d}^2 N_{\rm f} \frac{\beta_1 \sqrt{\gamma_1}}{\gamma_1^7} (I_1(x) + I_2(x) + I_3(x)).$$

The complete  $f_{2\gamma}(x)$  is obtained by summing over the  $f_{2\gamma}$  with different values of

<sup>\*)</sup> The percentages of the calculated two-photon energy distributions (figs. 1 and 2) falling within these ranges are 64 %, 94 % and 53 % respectively.

b) Ref. 19).
c) Ref. 17).
d) Ref. 18) and present work.

 $\beta$ ,  $\beta'$  and  $\gamma$  and the appropriate signs. The dimensionless function  $I_i(x)$  arises from the contribution of the term  $h_i$ . We have

$$\begin{split} I_{1}(x) &= -\frac{\gamma_{1}^{7}}{\pi\gamma^{4}} \int_{0}^{\infty} \frac{q^{2}\mathrm{d}q}{(q^{2} + \beta^{2})(q^{2} + \beta^{2})(q^{2} + \xi_{1}^{2})} + \frac{3\gamma_{1}^{7}}{2\pi\gamma^{2}} \int_{0}^{\infty} \frac{q^{4}\mathrm{d}q}{(q^{2} + \beta^{2})^{2}(q^{2} + \beta^{2})^{2}(q^{2} + \xi_{1}^{2})} \\ &- \left[ \frac{4a_{2}\gamma_{1}^{7}}{9\pi^{2}} \left\{ \frac{4}{9} \int_{0}^{\infty} \frac{q^{2}\mathrm{d}q}{(q^{2} + \beta^{2})(q^{2} + \beta^{2})} \int_{0}^{\infty} \frac{\mathrm{d}Q}{(Q^{2} + \gamma^{2})^{2}(Q^{2} + \xi_{2}^{2})} \right. \\ &+ \int_{0}^{\infty} \frac{q^{4}\mathrm{d}q}{(q^{2} + \beta^{2})^{2}(q^{2} + \beta^{2})^{2}} \int_{0}^{\infty} \frac{\mathrm{d}Q}{(Q^{2} + \gamma^{2})(Q^{2} + \xi_{2}^{2})} \right] ; \\ &+ \int_{0}^{\infty} \frac{q^{4}\mathrm{d}q}{(q^{2} + \beta^{2})^{2}(q^{2} + \beta^{2})^{2}} \int_{0}^{\infty} \frac{\mathrm{d}Q}{(Q^{2} + \gamma^{2})(Q^{2} + \xi_{2}^{2})} \right] ; \\ &+ 2(x) = -\frac{4\gamma_{1}^{7}}{\pi} \int_{0}^{\infty} \frac{q^{2}\mathrm{d}q}{(q^{2} + \beta^{2})(q^{2} + 4\beta^{2})(q^{2} + \gamma^{2})^{2}(Q^{2} + \xi_{2}^{2})} \\ &+ \frac{2048a_{2}\gamma_{1}^{7}}{(27\pi^{2})^{2}} \left[ \int_{0}^{\infty} \frac{q^{2}\mathrm{d}q}{q^{2} + \beta^{2}} \int_{0}^{\infty} \frac{4\mathrm{d}Q}{(Q^{2} + \xi_{2}^{2})(Q^{2} + \xi_{3}^{2})^{2}(Q^{2} + \xi_{4}^{2})} \\ &\times \left\{ \frac{1}{3} + \frac{q^{2}}{q^{2} + \beta^{2}} - \left( \frac{8}{3}q^{2} + \frac{2q^{2}Q^{2}}{q^{2} + \beta^{2}} \right) \left( \frac{2}{Q^{2} + \xi_{3}^{2}} - \frac{1}{3(Q^{2} + \xi_{4}^{2})} \right) \right\} \right], \\ \text{where } \xi_{1}^{2} = \gamma_{1}^{2}x + \beta^{2}, \ \xi_{2}^{2} = \frac{4}{3}(q^{2} + \xi_{1}^{2}), \ \xi_{3}^{2} = 4(q^{2} + \gamma^{2}) \text{ and } \xi_{4}^{2} = \frac{4}{9}(q^{2} + 4\beta^{2}); \\ I_{3}(x) = -\frac{2\gamma_{1}^{7}}{\pi} \int_{0}^{\infty} \frac{q^{2}\mathrm{d}q}{(q^{2} + \xi_{1}^{2})(q^{2} + \beta^{2})(q^{2} + 4\beta^{2})(q^{2} + \gamma^{2})} \\ &\times \left\{ \frac{1}{q^{2} + \gamma^{2}} + \frac{15}{q^{2} + 4\beta^{2}} - \frac{6\beta^{2}}{(q^{2} + \beta^{2})(q^{2} + 4\beta^{2})} - \frac{2\beta^{2}}{(q^{2} + \beta^{2})(q^{2} + \gamma^{2})} \right\} \\ &+ \frac{2048a_{2}\gamma_{1}^{7}}{27\pi^{2}} \int_{0}^{\infty} \frac{q^{2}\mathrm{d}q}{(q^{2} + \beta^{2})} \left[ \frac{1}{9} \int_{0}^{\infty} \frac{\mathrm{d}Q}{(Q^{2} + \xi_{2}^{2})(Q^{2} + \xi_{3}^{2})} \right] \\ &\times \left\{ \frac{3}{4} - \frac{3}{8} \frac{\beta^{2}}{q^{2} + \beta^{2}} - \frac{1}{3} \left( q^{2} + \frac{9}{4} \frac{q^{2}Q^{2}}{q^{2} + \beta^{2}} \right) \left( \frac{1}{3(Q^{2} + \xi_{4}^{2})} - \frac{1}{Q^{2} + \xi_{3}^{2}} \right) \right\} \\ &+ 4 \int_{0}^{\infty} \frac{\mathrm{d}Q}{(Q^{2} + \xi_{2}^{2})(Q^{2} + \xi_{2}^{2})(Q^{2} + \xi_{3}^{2})^{2}}{(q^{2} + \beta^{2})^{2}} \left( \frac{1}{3(Q^{2} + \xi_{4}^{2})} - \frac{1}{Q^{2} + \xi_{3}^{2}} \right) \left( \frac{1}{3(Q^{2} + \xi_{4}^{2})}$$

In evaluating the above expressions, the following integrals have been used,

$$\int_0^\infty \frac{\mathrm{d}q}{(q^2 + \alpha^2)(q^2 + \beta^2)} = \frac{\pi}{2\alpha\beta(\alpha + \beta)},$$

# Appendix B

For a double E1,  $\frac{1}{2}^+ \rightarrow \frac{5}{2}^+$  transition,

$$\sum' |M_{2\nu}|^2 = \sqrt{\frac{1}{2}} 2\pi \sqrt{\omega_1 \omega_2} (1 + \frac{3}{10} \sin^2 \theta + \frac{2}{5} \cos^2 \theta) |R_{2\nu}(\omega_1) + R_{2\nu}(\omega_2)|^2, \quad (B.1)$$

where  $\theta$  is the angle between the two emitted photons and

$$R_{2\gamma}(\omega_1) = \sum_{n} \langle \frac{5}{2} || r || n; \frac{3}{2} \rangle \langle n; \frac{3}{2} || r || \frac{1}{2} \rangle / (E_n - E_0 + \omega_1), \tag{B.2}$$

where  $E_0$  ( $E_n$ ) is the energy of the initial (intermediate) nuclear state. We define a dimensionless amplitude f(x)

$$R_{2\gamma}(\omega_1) \equiv \sqrt{120\pi} N_f \gamma_1^{-4} \omega^{-1} (A/Z) f(x),$$
 (B.3)

where  $x = \omega_1/\omega$ , then

$$\frac{d\sigma_{2\gamma}}{d(\cos\theta)} = 20\bar{N}_{\rm f}^2 \frac{\alpha^2}{v_{\rm n}} \left(\frac{\omega}{2\mu}\right)^{\frac{1}{2}} \gamma_1^{-2} \left(\frac{Z}{A}\right)^4 F(\eta) (1 + \frac{3}{10}\sin^2\theta + \frac{2}{5}\cos^2\theta), \tag{B.4}$$

where

$$F(\eta) = 6 \int_0^1 |f(x) + f(1-x)|^2 x^3 (1-x)^3 dx.$$
 (B.5)

Integrating over  $\theta$  provides a factor of  $\frac{8}{3}$ , leading to eq. (16). For the amplitude  $f^{*,p}$ , the radial wave function of the initial scattering state (s'<sub>1</sub>) is

$$u_0(z) = \sqrt{4\pi} \left[ 1 - \frac{\eta}{z} (1 - e^{-\zeta z}) \right];$$
 (B.6)

where  $z = r\gamma_1$ , and  $\eta = a\gamma_1$ ; a is the scattering length. Asymptotically (r is greater

than the radius of the nucleus)

$$u_0(z) \rightarrow u_0^{\text{asym}}(z) = \sqrt{4\pi}(1 - \eta/z).$$

The radial wave function for the bound state  $(d_5)$  is  $N_f u_2$ . Asymptotically

$$u_2(z) \to u_2^{\text{asym}}(z) = \frac{e^{-z}}{z} \left( 1 + \frac{3}{z} + \frac{3}{z^2} \right).$$

The sum over the plane wave intermediate states is replaced by the integral  $[1/(2\pi)^3]\int d^3p$ , and  $E_n - E_0 = p^2/2\mu$ . Substituting into (B.2) and (B.3) we have (19). When we use the approximation  $u_2(z) = u_2^{asym}(z)$  and  $u_0(z) = u_0^{asym}(z)$  we have

$$f^{\text{asym}}(x) = \frac{1}{x} - \frac{4\eta}{15\pi} \int_0^\infty \frac{\mathrm{d}p}{p^2 + x} \left[ \frac{2}{(1+p^2)^2} + 2_2 F_1(\frac{3}{2}, 2; \frac{5}{2}; -p^2) + {}_2F_1(1, \frac{3}{2}; \frac{5}{2}; -p^2) \right], \quad (B.7)$$

where  ${}_2F_1$  is the hypergeometric function. The value for  $\sigma_{2\gamma}$  calculated with  $f^{\text{asym}}$  above is <sup>5</sup>) 36 nb, as compared to 41 nb when  $f^{\text{s.p.}}$  is used. When the scattering is weak, or  $\eta \approx 0$ , we have  $f^{\text{asym}}(x) \approx 1/x$  and  $F^{\text{asym}}(0) = 1$ , which explains our normalization of f(x) in (B.3) and  $F(\eta)$  in (B.5). In the present case the scattering is sufficiently strong (a = 5.81 fm,  $\eta = 2.52$ ) such that f(x) = 1/x is a poor approximation.

For the amplitude  $f^{GDR}$  we consider the contribution from the core-excited intermediate states  $|1^-d_5; \frac{3}{2}\rangle$  and  $|1^-s_1'; \frac{3}{2}\rangle$ . We get

$$R_{2\gamma}^{GDR}(\omega_1) = \frac{\langle \mathbf{d}_5 || \mathbf{r} || \mathbf{1}^{-} \mathbf{s}_1'; \frac{3}{2} \rangle \langle \mathbf{1}^{-} \mathbf{s}_1'; \frac{3}{2} || \mathbf{r} || \mathbf{s}_1' \rangle}{\omega_D + \omega_1} + \frac{\langle \mathbf{d}_5 || \mathbf{r} || \mathbf{1}^{-} \mathbf{d}_5; \frac{3}{2} \rangle \langle \mathbf{1}^{-} \mathbf{d}_5; \frac{3}{2} || \mathbf{r} || \mathbf{s}_1' \rangle}{\omega_D - \omega + \omega_1}$$
(B.8)

We expect the two terms (B.8) to be of comparable importance. Because only the first term can be easily estimated we equate  $R_{2\gamma}^{\rm GDR}$  to twice the first term. It is then easy to show that

$$\langle 1^{-}s'_{1}; \frac{3}{2} ||r||s'_{1} \rangle = \langle 1^{-} ||r||0^{+} \rangle \approx \frac{1}{\gamma_{D}} \left( \frac{NZ}{A} \right)^{\frac{1}{2}},$$
 (B.9)

where  $\gamma_D = \sqrt{2\mu\omega_D}$  and we have assumed that the GDR exhausts the dipole sum rule of Thomas-Reiche-Kuhn <sup>20</sup>). To calculate the other dipole matrix element in (B.8) we must express the GDR in terms of particle-hole components. We have

$$\langle \mathbf{d}_{5} || \mathbf{r} || 1^{-} \mathbf{s}'_{1}; \frac{3}{2} \rangle = \frac{y_{d}}{2\sqrt{2}} \langle 0^{+} || \mathbf{r} || (\mathbf{s}_{1} \mathbf{p}_{3}^{-1}) 1^{-} \rangle$$

$$= y_{d} \frac{Z}{A} \sqrt{\frac{2}{3}\pi} K \gamma_{1}^{-\frac{1}{4}}, \tag{B.10}$$

where  $p_3$  is a  $p_4$  hole,  $K = \int_0^\infty u_1(z)(1-\eta/z)z^3dz$ , and  $u_1$  is the normalized wave function

for  $p_3$ . Substituting (B.8)–(B.10) into (B.3) we get (20). Parameter K is calculated using the harmonic oscillator (length parameter b=1.76 fm) wave function, yielding K=1.78. For the excitation energy of the GDR we use  $\omega_D=22$  MeV. For the amplitude  $y_d$  we use the average value of  $y_d=\sqrt{\frac{1}{5}}$  as there are five major particle-hole components in the GDR of <sup>16</sup>O.

For the amplitude  $f^{2+}$  we again equate the contribution from the two possible terms to twice the term for which a simple calculation is feasible

$$R_{2\gamma}^{2+}(\omega_1) \approx 2 \frac{\langle 2^+ s_1'; \frac{5}{2} || r || 1^- s_1'; \frac{3}{2} \rangle \langle 1^- s_1'; \frac{3}{2} || r || s_1' \rangle}{\omega_D + \omega_1} \frac{\langle d_5 | V | 2^+ s_1'; \frac{5}{2} \rangle}{2\omega_D}, \quad (B.11)$$

where  $|2^+\rangle$  is the two-phonon state  $|1^-\otimes 1^-;2^+\rangle$  and V is the residual interaction. By vector recoupling we have

$$\langle \mathbf{d}_5 | V | 2^+ \mathbf{s}_1'; \frac{5}{2} \rangle = \sqrt{\frac{3}{2}} y_d \langle (\mathbf{s}_1' \mathbf{p}_3^{-1}) 1^- | V | 1^- \rangle.$$
 (B.12)

The last matrix element can be calculated simply if we assume  $V = \lambda r_1 \cdot r_2$ . Then it is easily shown that

$$3\lambda = \omega_{\rm D} \langle 1^- || \mathbf{r} || 0 \rangle^{-2},$$

and that

$$\langle (\mathbf{s}_{1}'\mathbf{p}_{3}^{-1})\mathbf{1}^{-}|V|\mathbf{1}^{-}\rangle = \sqrt{\frac{1}{3}}\omega_{\mathbf{D}}\langle 0^{+}||\mathbf{r}||(\mathbf{s}_{1}'\mathbf{p}_{3}^{-1})\mathbf{1}^{-}\rangle\langle 1^{-}||\mathbf{r}||0^{+}\rangle. \tag{B.13}$$

The first matrix element in (B.11) is

$$\langle 2^+ s_1'; \frac{5}{2} || \mathbf{r} || 1^- s_1'; \frac{3}{2} \rangle = 2 \langle 1^- || \mathbf{r} || 0^+ \rangle.$$
 (B.14)

From (B.11)-(B.14) we have

$$R_{2\gamma}^{2+}(\omega_1) \approx 2R_{2\gamma}^{GDR}(\omega_1),$$

and (21) follows.

#### References

- 1) D. P. Grechukhin, Sov. J. Nucl. Phys. 14 (1972) 62
- 2) M. Verde, Handbuch der Phys., vol. 39 (Springer Verlag, Berlin, 1957) p. 144
- E. D. Earle, A. B. McDonald, O. Hausser and M. A. Lone, Phys. Rev. Lett. 35 (1975) 908;
   E. D. Earle, A. B. McDonald and M. A. Lone, Phys. Rev. C14 (1976) 1298, and references quoted therein
- J. Blomqvist and T. E. O. Ericson, Phys. Lett. 61B (1976) 219;
   H. C. Lee and F. C. Khanna, Phys. Lett. 61B (1976) 216; Phys. Rev. C14 (1976) 1306, and references quoted therein
- 5) H. C. Lee, F. C. Khanna, M. A. Lone and A. B. McDonald, Phys. Lett. 65B (1976) 201
- 6) D. P. Grechukhin, Nucl. Phys. 35 (1962) 98
- 7) Y. E. Kim and A. Tubis, Ann. Rev. Nucl. Sci. 24 (1974) 69
- 8) A. Laverne and C. Grignoux, Nucl. Phys. A203 (1973) 59
- 9) L. Hulthén and M. Sugawara, Handbuch der Physik, vol. 39 (Springer Verlag, Berlin, 1957) p. 1
- 10) F. C. Khanna, Nucl. Phys. A165 (1971) 475;
  - L. M. Delves and A. C. Phillips, Rev. Mod. Phys. 41 (1969) 497

- 11) S. Kahana, H. C. Lee and C. K. Scott, Phys. Rev. 180 (1969) 956
- 12) D. J. Hughes and R. B. Schwartz, Neutron cross sections, BNL-325, 2nd ed. (USAEC, 1958)
- 13) P. Spilling, H. Guppelaar, H. F. DeVries and A. M. J. Spits, Nucl. Phys. A113 (1968) 395
- 14) D. Bellman, Atomkernenergie 17 (1971) 145
- 15) E. T. Jurney, quoted in F. Ajzenberg-Selove and T. Lauritsen, Nucl. Phys. A227 (1974) 1
- 16) H. C. Lee and E. D. Earle, Nucl. Instr. 131 (1975) 199
- 17) S. Fiarman and S. S. Hanna, Nucl. Phys. A251 (1975) 1
- E. T. Jurney and H. T. Motz, Proc. Int. Conf. on nuclear reactions with reactor neutrons, ed. F. E. Throw, ANL-6797 (1963) 236
- S. F. Mughabghab and D. I. Garber, Neutron cross sections, vol. 1, resonance parameters, BNL-325, 3rd ed. (USAEC, 1973)
- 20) J. S. Levinger, Nuclear photo-disintegration (Oxford University Press, London, 1960)